JOURNAL OF SPACECRAFT AND ROCKETS
Vol. 42, No. 1, January–February 2005

Optimal Design of Two-Stage-to-Orbit Space Planes with Airbreathing Engines

Takeshi Tsuchiya*
University of Tokyo, Tokyo 113-8656, Japan
and
Takashige Mori†
Japan Aerospace Exploration Agency, Tokyo 182-8522, Japan

Many candidate concepts of reusable space transportation vehicles have been proposed around the world. Our aim in this study is to apply an optimization method for conceptual designs of two-stage-to-orbit (TSTO) space planes with airbreathing engines on the first-stage boosters and to obtain necessary vehicle sizes and their optimal flight trajectories. First, we integrate analysis methods into the optimization problem, the solution of which yield the minimized total dry mass of the first-stage booster and the second-stage orbiter. This information allows us to determine the optimal vehicle configuration and flight trajectory for a highly feasible TSTO space plane. The optimal solutions show that TSTO space planes with boosters powered by rocket engines added to the airbreathing engines are lighter in total dry mass than vehicles with boosters propelled by only airbreathing engines. However, it is necessary to lighten and miniaturize vehicle components to achieve greater feasibility. In addition, the trajectory optimizations enable the booster to glide back to a launch site using little propellant, despite the long downrange path from the staging point of the ascent trajectory. This study confirms that the analysis and optimization method proposed are effective.

Introduction

AS an effort toward new space transportation system development, while aiming to further improve the technical levels of expendable rockets, space development agencies around the world have been studying reusable launch vehicles (RLVs), which aim at reduced operation cost and improved reliability. Although the United States is an overwhelming leader in this field, as we all know, Japan has also consistently contributed new flight technologies, as demonstrated by OREX (orbital reentry experiment), HYFLEX (hypersonic flight experiment), ALFLEX (automatic landing flight experiment), and HSFD (high-speed flight demonstration).[1] The Japan Aerospace Exploration Agency (JAXA) and its three predecessor agencies (National Space Development Agency, National Aerospace Laboratory, and Institute of Space and Astronautical Science) have taken the lead nationally in the study of winged horizontal takeoff and landing space planes with new types of airbreathing engines running at hypersonic speed. Various types of engines have also been studied.[2,3] In June 2000, the Committee on Future Space Transportation Systems, established within Japan's Science and Technology Agency, defined a new direction for Japan's space transportation systems in the 21st century: an incremental research and development program whose final goal is a single-stage-to-orbit space plane, with an interim fully reusable two-stage-to-orbit (TSTO) space plane to be developed within a few decades.[4] On the basis of that directive, Japan has begun conceptual studies of TSTO systems. The authors have also conducted the research to verify the vehicle specification in Ref. 4.

Conceptual designs of space launch vehicles are difficult because they cannot be conducted without the cooperation of numerous disciplines that incorporate several analysis technologies, including aerodynamics analysis, heating analysis, structural analysis, propulsion analysis, trajectory analysis, controls analysis, cost analysis, operations analysis, and so on. As a reusable space transportation system is realized only at frontiers of the present technologies, it is necessary to make efficient use of the analysis technologies in the disciplines and to apply optimization techniques. The application of optimization methods to multidisciplinary analysis is referred to as multidisciplinary design optimization (MDO). With advances in computers, various MDO methods have been applied widely to designs of aircrafts and space transportation vehicles.[5]

Based on the studies of RLVs using MDO, our previous paper[6] dealt with conceptual design problems of rocket TSTO vehicles, in which multiple analysis methods were integrated and optimal designs of the TSTO vehicles were developed using an optimization method. A purpose of the present paper is to apply these methods to TSTO space planes with airbreathing engines. The TSTO space plane discussed here, which takes off and lands horizontally, is comprised of two winged-body vehicles: a first-stage booster and a second-stage orbiter, as indicated in Ref. 4. Though the reference envisions the booster with only airbreathing engines, we also consider installing rocket engines in addition to the airbreathing engines on the booster. These two styles of space plane, with different payload capabilities, are optimized in the same manner for comparison. Trajectory optimization characterizes the optimization problems in this paper. We optimize three-degree-of-freedom trajectories in addition to optimizing the other design parameters. The results show some examples of highly feasible TSTO space plane designs. Finally, we make a comparison between the present results and the rocket TSTO vehicles described in Ref. 6.

Analysis Method and Optimization Problem

The TSTO space plane in this study is made up of a first-stage booster and a second-stage orbiter, which are shown in Fig. 1. This figure also indicates the geometric parameters that we have to specify. The other design variables are flight performance parameters and flight trajectory variables, which are given by Table 1. In this study we optimize ascent and return trajectories; the design variables contain state and control variables of the flight trajectories.

Figure 2 shows the analysis process. Each analysis calculates output values for the subsequent analysis from the values of design variables and the input values obtained from the previous analysis.

Received 2 February 2004; revision received 4 April 2004; accepted for publication 5 April 2004.

*Lecturer, Department of Aeronautics and Astronautics; tsuchiya@mail.ecc.u-tokyo.ac.jp. Member AIAA.

†Senior Researcher, Future Space Transportation Center, Chofu. Member AIAA.

Table 1 Design variables of vehicle configuration and flight trajectory

Parameter type	Variable
Booster's geometry (Fig. 1)	$l_1, l_2, l_3, l_4, D, C_r, C_t, b$
Orbiter's geometry (Fig. 1)	$l_0, l_1, l_2, l_3, D, C_r, C_t, b$
Flight performance of booster	Gross mass
	Maximum body normal acceleration
	Maximum body axial acceleration
	Maximum dynamic pressure
	ABE air capture area
	ABE maximum thrust
	RE thrust (vacuum)
Flight performance of orbiter	Gross mass
	Maximum body normal acceleration
	Maximum body axial acceleration
	Maximum dynamic pressure
	RE thrust (vacuum)
Flight trajectory	Discretized state variables
	Discretized control variables
	Initial times of subphases
	Terminal times of subphases

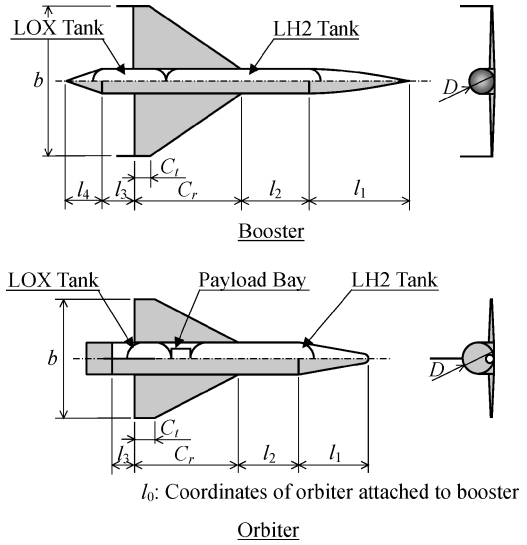

Fig. 1 Booster and orbiter layout.

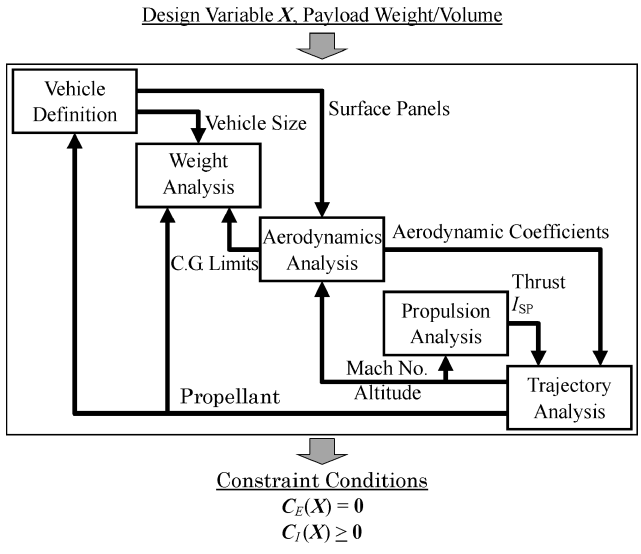

Fig. 2 Analysis process.

In addition, it computes the function values of equality and inequality constraint conditions ($\boldsymbol{C}_E$ and $\boldsymbol{C}_I$ in Fig. 2), which the design variables of the completed vehicle must satisfy. Though the values we find for the design variables must satisfy all of the constraint conditions, we cannot always obtain unique values. Therefore, we give a figure of merit and define an optimization problem to find the best values under the criterion. The following paragraphs provide brief descriptions of the analysis methods, constraint conditions, and a figure of merit in the optimization problem.

Vehicle Definition

The booster is derived from a wing-body hypersonic transportation vehicle. In contrast, the orbiter, which can reach orbit and reenter the atmosphere, is shaped like the Space Shuttle Orbiter of the U.S. and HOPE-X[7] of Japan. In this paper we consider two types of TSTO vehicles for the booster's propulsion system. One has the booster with only airbreathing engines for ascent and acceleration (hereafter the ABE booster or ABE vehicle). The other has the booster with rocket engines in addition to the airbreathing engines (hereafter the ABE/RE booster or ABE/RE vehicle). We select a precooled turbojet (PCTJ) engine as the airbreathing engine, the performance of which is detailed in the propulsion analysis later in this paper. The airbreathing engines are suspended on the undersurface of the wings, and the rocket engines of the booster and orbiter are installed in the aft fuselage. The number of engines is one of the design variables; however, the optimization method in this paper can only optimize continuous variables and not a discrete number of integer variables. Thus, we assign minimum numbers on the realistic condition that the thrust force per rocket engine is less than 1.5 MN and an air capture area of the airbreathing engine is below 6 m^2. This is because it is presumed in the weight analysis that having a small number of engines reduces the total engine mass. The fuselages of the booster and orbiter have nonintegral tanks for the required cryogenic propellant: liquid oxygen (LOX) and liquid hydrogen (LH2). Between the tanks of the orbiter is a cubic bay area for payloads, of which the mass and volume requirements are specified in the problem definition. The orbiter and booster have a vertical tail fin and tipfins, respectively, whose sizes are calculated based on the tail volume of HOPE-X. The area of a body flap of the orbiter is also based on the design of HOPE-X.

The vehicle definition generates surface panels for each of the vehicles from the geometric parameters. The panels' coordinate values and their attribution to either the fuselage or the wings are submitted to the aerodynamics analysis. In addition, the vehicle element sizes that are not included in the design variables are calculated for the weight analysis. To attain the proper vehicle shape, we compute inequality constraints for the geometric parameters. We also constrain the maximum values of acceleration and dynamic pressure in the ranges of 2.5–4 g and 15–50 kPa, respectively. At the same time, the trajectory analysis gives the amount of propellant, and the vehicle definition calculates the tank sizes accordingly. Some constraint conditions demand that the booster fuselage should be large enough to hold the tanks and that the orbiter fuselage should contain both the tanks and payload bay.

Aerodynamics Analysis

The aerodynamics analysis estimates the vehicles' aerodynamic properties using the surface panels of each vehicle as provided by the vehicle definition and tabulates lift and drag coefficients for typical angles of attack and Mach numbers from subsonic to hypersonic speed. These results are used to compute the flight trajectories. Another important operation of the aerodynamics analysis is to evaluate the longitudinal static stabilities from the pitching moments of the vehicles and find the aft limits of the centers of gravity (c.g.). We presume that the c.g. forward limits are 10% of body length forward of the aft limits.

For the aerodynamics analysis methods, we employ a panel method[8] in subsonic flight. The Prandtl–Meyer expansion flow theory and a tangent cone/wedge method are applied at supersonic to hypersonic speed. In addition, the base drag of the vehicle that has a cutoff aft fuselage is estimated from its base area and the Mach

number.[9] We also compute the skin-friction drag by the sum of the frictions that are obtained from the flow velocities on the panels. Transonic aerodynamic forces result from subsonic and supersonic forces, as explained in Ref. 9. The simple methods in this study are applicable to each vehicle separately and not to the coupled vehicle of the booster and orbiter. We presume that the coupled vehicle's lift force is equal to that of the booster and that its drag force is the sum of the total drag of the booster and the parasite drag of the orbiter. This means the study does not consider the interference drag caused by the coupling of the two vehicles. These simple and low-fidelity methods are useful in that they need a short computation time in the much iterative optimization process.

Propulsion Analysis

Given a flight altitude and Mach number by the trajectory analysis, the propulsion analysis calculates thrust forces and specific impulses of the airbreathing engine and the rocket engine. In this study, a PCTJ engine[3] is selected as the airbreathing engine. The PCTJ engine is one of the candidates for hypersonic engines; it can work up to about Mach 6 cruise. The PCTJ engine has a precooling heat exchanger in front of a turbojet engine to reduce the air temperature by the cooling capacity of liquid hydrogen. The air condition at Mach 6 through the heat exchanger is almost equivalent to that at Mach 3. The precooling also increases the air density. Then, thrust of the turbojet engine is largely increased. To enhance the precooling effect, fuel-rich operation is used, which also increases the thrust, even with a little loss of the specific impulse. We acquired the properties of the PCTJ engines from the Future Space Transportation Center of JAXA. Figures 3 and 4 provide the values of the thrust force per air capture area and the specific impulse in response to Mach number and altitude. The air capture area is one of the design variables, to which the thrust force generated by one engine is proportional. In this study, the engines are located on the wings, but air compression by the forebody of the booster is not considered.

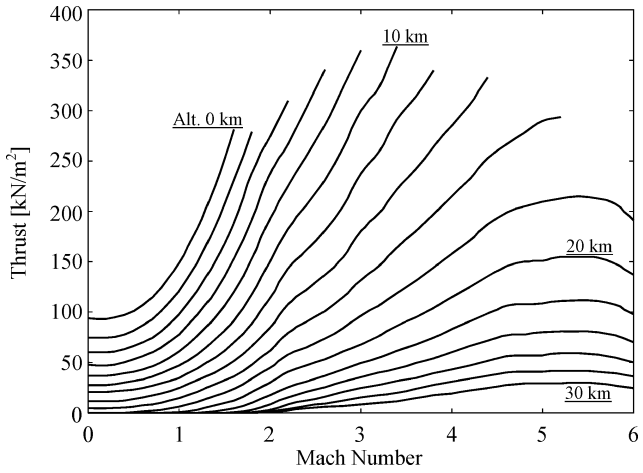

Fig. 3 Thrust force per air capture area of PCTJ engine.

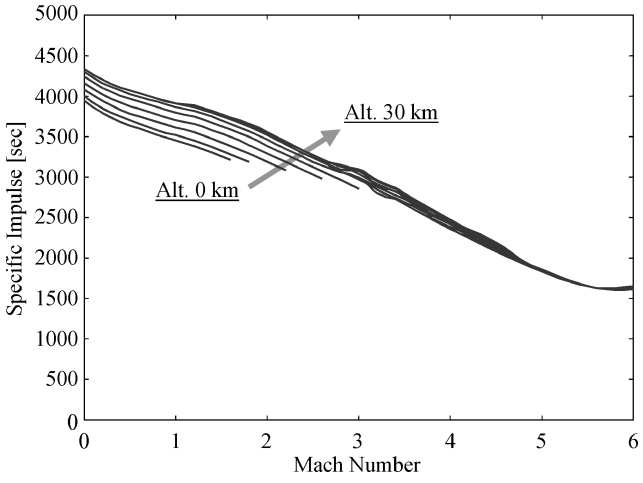

Fig. 4 Specific impulse of PCTJ engine.

The rocket engine uses cryogenic propellant (LOX/LH2). In this study we consider a conventional rocket engine given by historical perspective and not a specific engine. A thrust force $T_{\mathrm{RE_{inf}}}$ (Newtons) per engine in vacuum is one of the design variables. According to existing or developed rocket engines, we presume that a cross-section area of the rocket nozzle exit A_e (square meters) is proportional to $T_{\mathrm{RE_{inf}}}$, as expressed here:

$$A_e = 2.771 \times 10^{-6} T_{\mathrm{RE_{inf}}} \tag{1}$$

The atmospheric pressure p (pascals) changes the thrust force to T_{RE} (newtons) in the air:

$$T_{\mathrm{RE}} = K T_{\mathrm{RE_{inf}}} \tag{2}$$

$$K = 1 - pA_e \big/ T_{\mathrm{RE_{inf}}} \tag{3}$$

Simultaneously, a specific impulse I_{sp} (seconds) in the atmosphere is provided by the specific impulse $I_{\mathrm{sp_{inf}}}$ (seconds) in vacuum (fixed to be 445 s in this paper) and the preceding parameter K:

$$I_{\mathrm{SP}} = K I_{\mathrm{SP_{inf}}} \tag{4}$$

Weight Analysis

The weight analysis computes the component masses of the booster and orbiter from the geometric and flight performance parameters in the design variables, the component sizes given by the vehicle definition, and the amount of the propellants provided by the trajectory analysis. In this study we employ the HASA (Hypersonic Aerospace Sizing Analysis) program,[10] a statistical mass estimation method, with the following modifications:

1) The HASA program calculates landing-gear mass on the basis of gross mass. However, the orbiter uses its landing gear only for landing, not launching. The landing mass of the orbiter is much lighter than the gross mass because the propellant mass occupies a high proportion of the gross mass. Thus, we calculate the landing-gear mass of the orbiter based on its maximum landing mass.

2) We added a reaction control system, orbital maneuvering engines (RCS/OME), and their propellants, which the HASA program does not include, to the orbiter.

3) We presume that the nose edge and wing leading edges of the orbiter are provided with carbon–carbon material. Thermal protection materials equivalent to 30-mm-thick ceramic tiles are bonded to the other surfaces of the orbiter and to the booster's total surface.

4) The propellant tanks are made of aluminum alloy, and each is composed of a cylinder whose ends are dome shaped. We compute the tank mass from the tank wall thickness, which is obtained considering its working pressure, the masses of spot welds, sensor attachments, and so on.

5) We derived the equation to obtain rocket-engine masses from Ref. 11. As an example, a rocket engine with a maximum thrust force of 1.5 MN approximates a thrust-to-weight ratio of 65. For the airbreathing engine, the mass W_{ABE} (kilograms) is given as

$$W_{\mathrm{ABE}} = 1701.345A_c + 136.275A_c^{0.9850} + 1043.530A_c^{0.5834} + 178.744A_c^{0.2940} \tag{5}$$

where A_c (square meters) is the air capture area. The equation estimates the total mass of the components of the engine whose air capture area is below 6 m^2.

The estimation of the component masses needs the gross mass, which is the sum total of the component masses. For example, the landing-gear mass of the booster, as part of the gross mass, is expressed as an equation with a variable of the gross mass. Thus, the method analyzes the masses using the gross mass in the design variables to obtain the gross mass. We define an equality constraint condition that both the masses correspond exactly.

Component allocation in the vehicle makes it possible to compute a c.g. location. The flight situations define the constraint conditions by which the c.g. locations remain within the limits determined by the aerodynamics analysis. There is also an equality constraint condition that the c.g. location of the booster does not move when the orbiter is released from the booster. This implies that, in this simulation, the unchanging c.g. location determines the attachment location of the orbiter.

Trajectory Analysis

In this study we implemented three-degree-of-freedom (DOF) trajectory analysis.[12] As just described, we optimized the flight trajectory with the other design variables. The trajectory analysis must deal with dynamic variables (the state and control variables) that depend on time, while the other design variables are static and independent of time. Therefore, we discretized these variables to transform them into static variables like the other design variables.[13] In the same manner, we also discretized constraint conditions and the motion equations expressed as differential equations, which are functions of the state and control variables. The number of discrete elements was fixed at 200 in this study. A characteristic of the trajectory optimization is to optimize terminal times of the trajectories besides the state and control variables. This means that a staging Mach number and cutoff Mach numbers of ABE and RE are optimized.

The flight styles of the vehicles change the equations of motion. This divides the flight trajectory into four phases, as described next. In addition, if each vehicle flies with multiple engines, the engines are cut off one after another. Because the equations of motion change discontinuously at the shutdown points, we subdivided the phases into some intervals, referred to as subphases in this paper. We defined equality constraint conditions to make the time and variables equal between a series of subphases. The phases are explained as follows:

1) The booster ascent phase indicates the flight from the horizontal takeoff of the coupled vehicle until the orbiter separates from the booster. As our hypothetical launch site, we chose Aeon Airfield (Long. 157.36° West and Lat. 1.78° North) on Christmas Island of the Republic of Kiribati. After takeoff, having no bank angle, the coupled vehicle rises and accelerates east. The vehicle has constraint conditions involving the angle of attack, throttle, dynamic pressure, thrust, body normal acceleration, and body axial acceleration. The values for these are limited to the maximum values in the design variables, except for the angle of attack and the throttle of the rocket engines, which are below 20 deg and above 60%, respectively. The airbreathing engines can change the throttle, ranging from 0 to 100%.

In this study we consider two booster propulsion systems: the ABE booster and the ABE/RE booster. The ABE booster has only one subphase in this phase. In contrast, the ABE/RE booster has a subphase for the airbreathing engines and the subsequent subphases for the rocket engines. The number of the subphases in the rocket flight corresponds to the number of the rocket engines.

2) In the orbiter ascent phase the released orbiter accelerates with its rocket engines and climbs to an altitude of 120 km. At that altitude, the orbiter cuts off the rocket engines temporarily and zooms up with no thrust in an elliptical orbit whose apogee altitude is 200 km. Finally, an apogee kick puts the orbiter into a 200 km circular low Earth orbit (LEO).

At the beginning of this phase, the angle of attack is allowed to have discontinuous values with the terminal angle of attack of the booster in the previous phase. The bank angle remains 0 deg for the orbiter to fly east. The constraint conditions in this phase are the angle of attack, throttle, dynamic pressure, thrust, normal acceleration, and body axial acceleration. Their values are limited to the orbiter's flight performance parameters in the design variables, except for the angle of attack kept below 20 deg and the throttle ranging from 60 to 100%.

3) In the booster flyback phase, after releasing the orbiter, the booster turns to fly back to the launch site, Aeon Airfield. The airbreathing engines can propel the booster if necessary. Even the ABE/RE booster is allowed to use the airbreathing engines. The reason is that the return flight is probably a cruise flight, where the airbreathing engines can consume less propellants than the rocket engines. The bank angle, which until now has been fixed at 0 deg, is allowed to be free. The initial angle of attack must be equal to the terminal angle in the booster ascent phase. As in the ascent phase, the angle of attack, throttle, dynamic pressure, thrust, normal acceleration, and body axial acceleration are constrained in this phase. The terminal constraint conditions are that the latitude and longitude of the booster must be identical with those of the launch site and the altitude is zero.

4) In the orbiter reentry and return phase, after the orbiter completes its missions in orbit, the orbiter carrying a payload to the ground reenters the atmosphere and lands at the launch site. This phase does not compute the return trajectory of three DOF as the other phases do, and we only define some constraint conditions to examine whether the orbiter has feasible flight conditions within the limits of the equilibrium glide, heat rate, normal acceleration, and dynamic pressure.[14] The heat rate is limited to 400 kW/m^2 on the nose tip and the wing leading edges, while the normal acceleration and dynamic pressure limits are given by the design variables. In addition, the following constraint conditions are in effect: the lift-to-drag ratio of the orbiter at subsonic speed must be greater than five, which is equivalent to that of HOPE-X,[15] and the orbiter can pull itself up at the maximum angle of attack during landing flare without violating the body normal acceleration limit.

Optimization Problem

In addition to the design variables and constraint conditions just described, the total dry mass of the booster and orbiter is defined as a minimized parameter. As the dry mass has a strong relationship to the development cost, we explore the feasibility of TSTO space planes on the basis of that mass. In this study we compute the optimal solutions for the ABE and ABE/RE vehicles, in which three sets of payload masses and volumes are delivered to/from orbit: 0 Mg and 0 m^3, 4 Mg and 40 m^3, and 8 Mg and 80 m^3; hence, we consider six cases.

A sequential-quadratic-programming method is employed as an optimization method. There are more than 1000 optimized design variables. The reason for the large number is that they have not only the geometric and flight performance parameters, but also the discretized state and control variables, as explained in the preceding subsections.

Optimal Solutions

Optimal Vehicle Sizes and Configurations

Figure 5 compares mass configurations of the ABE and ABE/RE vehicles that have the specified payload masses and volumes. Tables 2 and 3 detail the component masses as well as the size and performance data for the vehicles. Even if the orbiter has no

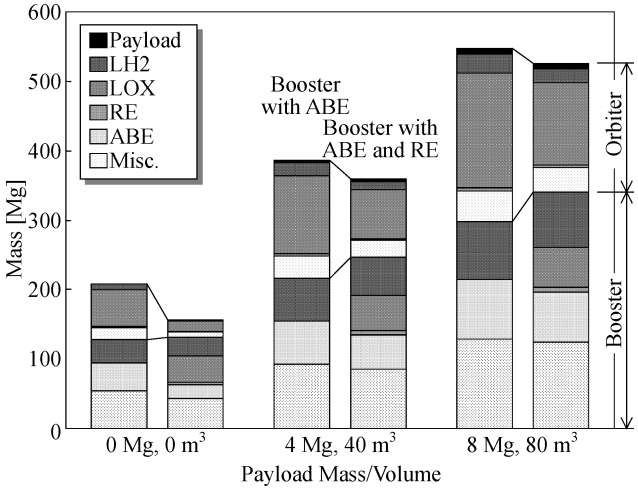

Fig. 5 Component mass comparison for the two booster styles.

Table 2 Performance and mass data of ABE vehicles

	Value for payload mass and volume					
	0 Mg and 0 m^3		4 Mg and 40 m^3		8 Mg and 80 m^3	
Parameter	Booster	Orbiter	Booster	Orbiter	Booster	Orbiter
Body length, m	74.69	29.99	89.75	41.45	99.11	43.64
Body diameter, m	3.74	3.46	4.49	4.47	4.96	5.59
Wing area, m^2	384.40	85.66	636.14	212.83	828.51	335.92
Maximum normal acceleration, *g*	2.5	2.5	2.5	2.5	2.5	2.5
Maximum axial acceleration, *g*	1.1	3.0	0.6	2.4	0.6	2.2
Maximum dynamic pressure, kPa	50.0	15.0	50.0	15.0	50.0	15.0
ABE total thrust, MN	2.28	——	2.68	——	3.70	——
ABE total engines	4	——	6	——	8	——
RE total thrust (vacuum), MN	——	0.96	——	2.06	——	3.00
RE total engines	——	1	——	2	——	3
Fuselage mass, Mg	12.71	3.83	18.28	7.04	22.79	9.01
Wing mass, Mg	8.05	0.86	15.56	2.06	22.81	3.40
Stabilizer mass, Mg	1.88	0.43	4.17	1.00	6.48	1.63
Thermal protection system (TPS) mass, Mg	5.75	2.34	9.22	4.64	11.92	6.54
Landing-gear mass, Mg	9.64	0.57	19.24	1.30	28.44	1.95
Tank mass, Mg	6.47	2.78	9.56	4.80	13.27	6.12
ABE mass, Mg	39.08	——	62.32	——	85.27	——
RE mass, Mg	——	1.57	——	3.33	——	4.88
Misc. mass, Mg	10.42	4.47	16.66	6.99	23.63	8.80
Dry mass, Mg	94.01	16.83	155.00	31.18	214.61	42.32
LH2 (ascent) mass, Mg	32.28	8.83	58.18	18.68	79.31	27.51
LH2 (return) mass, Mg	1.97	——	3.20	——	4.27	——
LOX mass, Mg	——	52.99	——	112.05	——	165.07
RCS/OME propellant mass, Mg	——	1.99	——	4.16	——	5.95
Gross mass, Mg	128.26	80.65	216.38	170.07	298.19	248.86

Table 3 Performance and mass data of ABE/RE vehicles

	Value for payload mass and volume					
	0 Mg and 0 m^3		4 Mg and 40 m^3		8 Mg and 80 m^3	
Parameter	Booster	Orbiter	Booster	Orbiter	Booster	Orbiter
Body length, m	56.83	22.62	76.43	33.37	95.65	38.17
Body diameter, m	3.97	2.28	4.66	4.47	4.83	5.59
Wing area, m^2	406.57	34.28	753.02	183.37	1067.30	302.07
Maximum normal acceleration, *g*	2.5	2.5	2.5	2.5	2.5	2.5
Maximum axial acceleration, *g*	2.7	2.9	1.4	2.5	1.0	2.5
Maximum dynamic pressure, kPa	50.0	15.0	50.0	15.0	50.0	15.0
ABE total thrust, MN	0.88	——	2.26	——	3.27	——
ABE total engines	2	——	4	——	6	——
RE total thrust (vacuum), MN	2.20	0.28	3.90	1.29	4.56	2.16
RE total engines	2	1	3	1	4	2
Fuselage mass, Mg	10.14	1.79	17.31	5.20	23.29	7.40
Wing mass, Mg	7.32	0.30	16.38	1.62	25.56	2.86
Stabilizer mass, Mg	1.21	0.09	3.01	0.92	4.63	1.60
TPS mass, Mg	5.05	1.07	9.17	3.83	12.83	5.79
Landing-gear mass, Mg	7.00	0.24	17.75	0.97	27.20	1.61
Tank mass, Mg	5.31	1.15	9.37	3.01	14.07	4.21
ABE mass, Mg	19.56	——	49.11	——	71.77	——
RE mass, Mg	3.54	0.54	6.11	2.03	7.29	3.48
Misc. mass, Mg	7.33	2.57	12.88	5.57	16.96	7.48
Dry mass, Mg	66.44	7.75	141.09	23.14	203.59	34.42
LH2 (ascent) mass, Mg	26.02	2.45	53.12	11.81	77.21	19.77
LH2 (return) mass, Mg	0.31	——	1.57	——	2.56	——
LOX mass, Mg	38.53	14.69	50.81	70.87	56.72	118.63
RCS/OME propellant mass, Mg	——	0.92	——	3.21	——	5.02
Gross mass, Mg	131.30	25.80	246.60	113.03	340.08	185.85

payload capability, the total dry masses of the ABE and ABE/RE vehicles are 110 and 74 Mg, respectively. An increase in the payload capacity by 1 Mg and 10 m^3 results in an increase in the total dry mass by more than 10 Mg. If the TSTO space planes are made to replace Japan's expendable H-IIA rocket, which can transport a payload of more than 10 Mg to LEO, the total gross masses will probably reach 600 Mg, whereas the H-IIA rocket weighs about 290 Mg. Compared with existent airplanes, the TSTO space planes are quite heavy.

The ABE/RE vehicles are lighter than the ABE vehicles in total dry mass and gross mass. The difference of the dry mass under the payload requirement in this study is 19 to 37 Mg; the rate to the dry masses of the ABE vehicles ranges from 7 to 33%. The difference is especially prominent in the vehicles with low payload capability. Though the mass difference becomes less with the increase of the payload capacity and vehicle size, the ABE/RE vehicles have lower dry and gross masses than the ABE vehicles under the payload capability studied in this paper because the airbreathing engines are heavy, accounting for 30–40% of the dry masses of the boosters. In spite of such heavy airbreathing engines, the thrust-to-weight ratio is five at best, whereas that of the rocket engine is 50–60. Reference 16 shows that this feature also is found in TSTO space planes

with different airbreathing engines than the PCTJ engines. If we install both the rocket engines and airbreathing engines in the booster, the mass of the rocket engines themselves is small, but the booster, which requires LOX as an oxidizer, is heavy. The orbiter, however, is lighter, as the increase in acceleration performance of the booster reduces the requirement of orbiter acceleration performance, as shown in flight histories in the following subsection. Thus the total dry and gross masses of the ABE/RE vehicles are smaller than those of the ABE vehicles. The small gross mass also generates a synergistic effect that makes airbreathing engines small. However, the estimation error of the weight analysis, HASA, in this paper can amount to 10% (Ref. 10). This means that TSTO space planes with the airbreathing and rocket engines do not always result in lightweight vehicles. Moreover, the ABE/RE vehicles can weigh more than these results because this study did not include incremental mass resulting from installing both of ABE and RE in a single vehicle. We need more accurate estimations of the component masses. In addition, though we explained that the smallest vehicle is the nearest to realization, mass is not the only criterion when candidate space transportation systems are narrowed down. We have to consider other criteria: cost, operability, reliability, and so on.

Figures 6 and 7 illustrate the boosters and orbiters designed based on the optimization results. The ABE/RE vehicles are a little smaller than the ABE vehicles, even with LOX. As the payload requirement increases, the difference between the two is smaller. The fuselage of the ABE/RE vehicle with no payload capability, which is the smallest vehicle, is 56.8 m long and 4.0 m wide. The vehicle with a payload capacity of more than 8 Mg and 80 m^3 exceeds 100 m long, which would pose operational problems insofar as the boosters would be bigger than existing airplanes and rockets. Thus, to increase the feasibility of these vehicles, the reduction of size as well as mass is essential.

The boosters have fine fuselages, and the fineness ratio of some boosters reaches 20, which is the maximum limit of the constraint

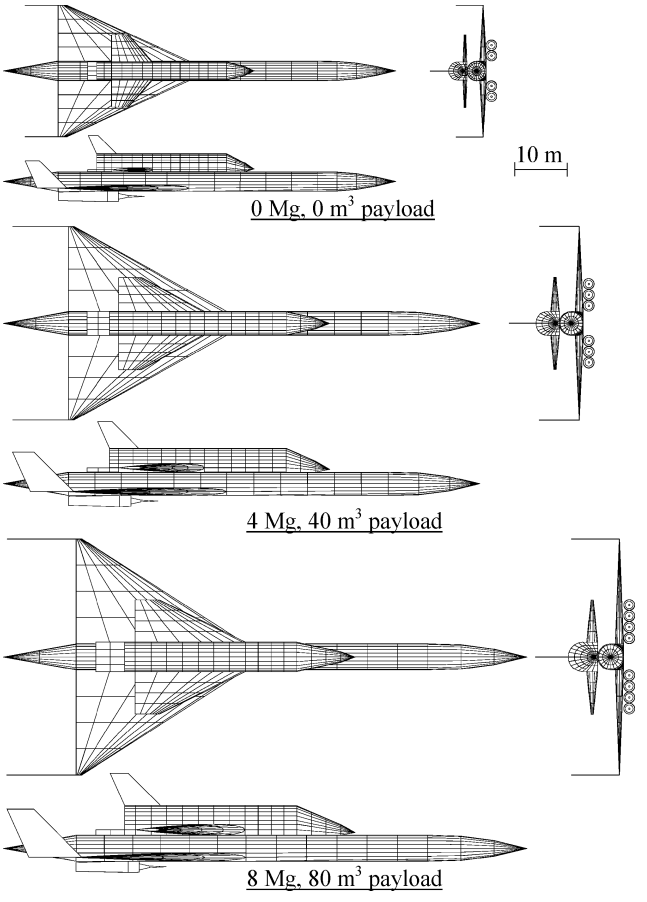

Fig. 6 Optimal ABE vehicles.

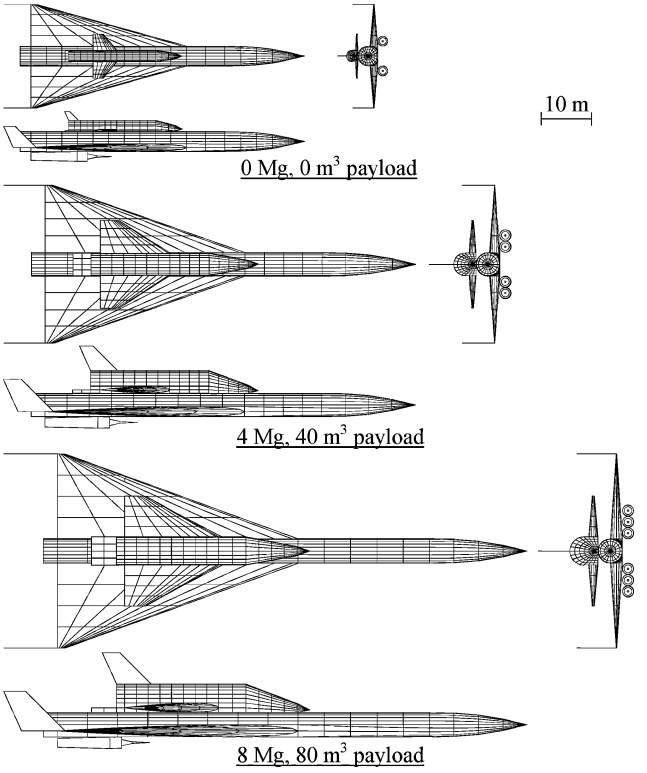

Fig. 7 Optimal ABE/RE vehicles.

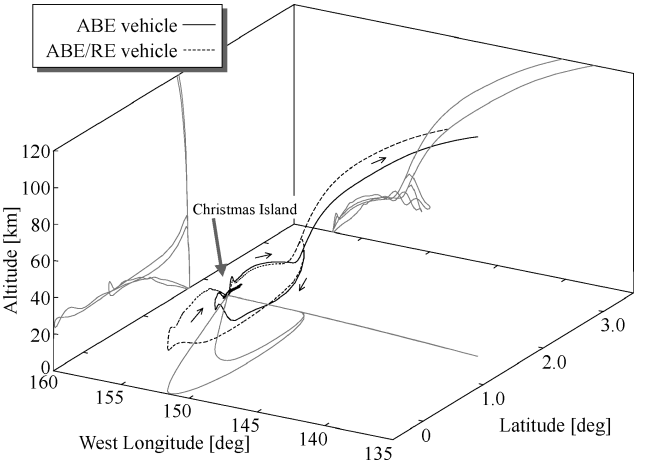

Fig. 8 Trajectory plots of ABE and ABE/RE vehicles (4 Mg and 40 m^3 payload).

condition. This is because the booster must fly back to the launch site and extend the reachable range by reducing the drag and increasing the lift-to-drag ratio. We still must examine issues such as body strength analysis and the feasibility of elongated propellant tanks, which have not been taken into consideration in this paper. Furthermore, the wings of the booster and orbiter have a small aspect ratio. The wing area of the booster coincides with the smallest area that allows the booster coupled with the orbiter to take off at the maximum angle of attack. On the other hand, the wing area of the orbiter depends on the flight conditions from reentry to landing, as the orbiter is subject to little aerodynamic force in its ascent flight after being released from the booster. These wings are at the limit size for vehicle flight, and wing loading of the vehicle obtained is larger than that of existent airplanes.

Optimal Flight Trajectories

Figures 8–11 show optimal ascent trajectories and boosters' return trajectories of the ABE vehicle and ABE/RE vehicle with the

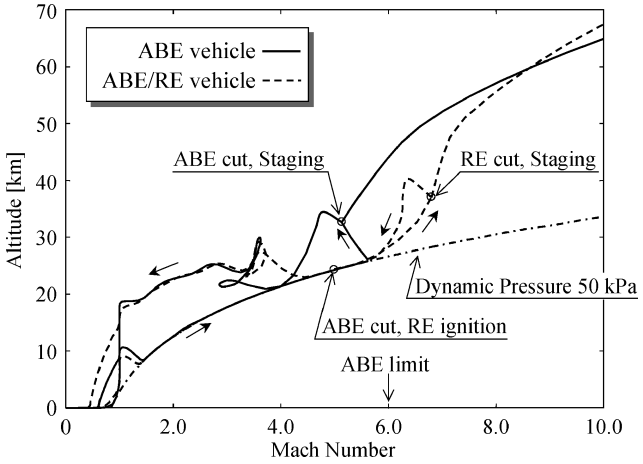

Fig. 9 Mach number and altitude histories of ABE and ABE/RE vehicles (4 Mg and 40 m^3 payload).

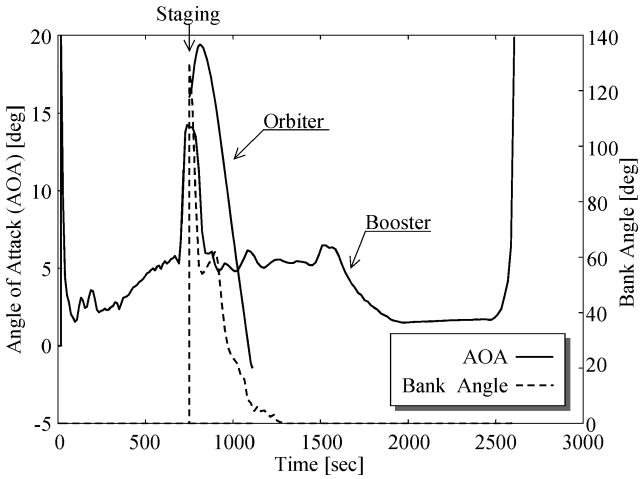

Fig. 10 Control history of ABE vehicle (4 Mg and 40 m^3 payload).

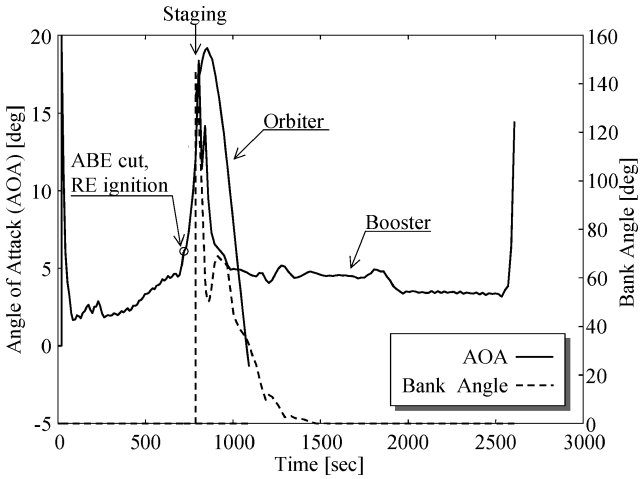

Fig. 11 Control history of ABE/RE vehicles (4 Mg and 40 m^3 payload).

4 Mg and 40 m^3 payload. Vehicles with different payload capabilities result in a variety of throttle controls and acceleration profiles from the different numbers of engines but exhibit about the same optimal flight trajectories and features.

When taking off, the ABE/RE vehicle has a thrust-to-weight ratio of 0.55, which is smaller than that of the ABE vehicle. It follows that the former glides over a runway in 1010 m, which is longer than the 860-m glide of the latter. Then the vehicles take off at the maximum angle of attack of 20 deg and increase their velocities and altitudes slowly. The maximum dynamic pressure limit of the booster's flight, which is one of the parameters optimized in the vehicle configurations, is 50 kPa because the higher dynamic pressure results in better performance of the airbreathing engines. The boosters, however, do not maintain the dynamic pressure of 50 kPa. The vehicles temporally hold the acceleration and climb to reduce the dynamic pressure in transonic speed, as shown in Fig. 9. The large size of the airbreathing engines, the aspects of which are explained in the preceding subsection, is needed for such transonic flight. In the range of supersonic and hypersonic speed, the vehicles fly all along the dynamic pressure of 50 kPa. For the ABE vehicle, when the booster reaches Mach 5.6, near the operation limit of the airbreathing engines, it increases the angle of attack to lose speed and gain altitude. The dynamic pressure decreases from 50 to 15 kPa, which is optimized as the maximum limit of the orbiter, and then the orbiter is released at 749 s, 32.7-km altitude, and Mach 5.1.

For the ABE/RE vehicle, the booster cuts off the airbreathing engines and ignites the rocket engines of the booster for further acceleration at Mach 5.0. The engine switch at lower Mach number is because the rocket engines provide a more fuel-efficient flight than the airbreathing engines over the Mach number. The rocket engines provide substantially constant efficiency in all circumstances, whereas the airbreathing engines become less efficient near the operation limit. The thrust-to-weight ratio of the booster's rocket engines approximates 1.3 at their ignition. After that, the ABE/RE vehicle continues to accelerate with the rocket engines, and then it releases the orbiter when it reaches 37.0 km altitude and Mach 6.8 (a dynamic pressure of 15 kPa) at 785 s. We need to examine whether it is possible for ABE and ABE/RE vehicles to release the orbiters at a high dynamic pressure such as 15 kPa.

The thrust-to-weight ratio of both of the orbiters' rocket engines right after the staging is about 1.2. The orbiters, constrained by the maximum acceleration limit, rise and accelerate by bang-bang throttle control to an altitude of 120 km. As we suppose that a thrust direction coincides with a body axis, the control of the angle of attack is equivalent to the thrust direction control in a low dynamic pressure environment.

Both the boosters fly 600–625 km away from the launch site, when separating from the orbiters. Just after the staging, the boosters shut all of the engines off for glide flights and start a turn with a bank angle that reaches 130–145 deg. At a high bank angle, the boosters gain a short turning radius but lose altitude and velocity. The optimization provides the best bank angle and angle of attack between the losses and gains. The boosters subtly adjust the two angles to prevent the dynamic pressure and body normal acceleration from exceeding the optimized limits. Crossranges of the ABE and ABE/RE boosters in the turn flights reach 145 and 250 km, respectively. The reason the latter is larger is that the separation altitude and speed of the ABE/RE boosters are larger than those of the ABE boosters. As the ground projection of the flight path points to the launch site, the boosters gradually lessen the bank angle and the angle of attack. The boosters ignite the airbreathing engines only in several tens of seconds to compensate for the lack of the required flight range to the launch site when the Mach number is approximately 3.5. As the bank angle is almost 0 deg, the angle of attack is set to that which maximizes the lift-to-drag ratio. This extends the flight range and enables the boosters to glide back to the launch site. The booster flight performances are optimized to allow the boosters to return to the launch site in such a flight. The characteristics of the optimal return trajectories are the nonlevel turn just after the staging, the long glide flight, and the brief ignition of the airbreathing engines. Less than 5% of the total propellant is required to fly back to the launch site, even in the long downrange.

Comparison to Rocket Launch TSTO Vehicles

In Ref. 6, we demonstrated the conceptual studies of winged rocket TSTO vehicles using an optimization technique. The analysis method in that study was the same as that used in this paper, while a minimized parameter is a gross mass. Reference 6, however, describes that, for rocket vehicles with hydrogen-oxygen propellants,

the dry mass and the gross mass are closely linked, and the sizes and masses of the optimal vehicles in both cases of minimized parameters differ by not more than 10%. Therefore, it is possible to compare the airbreathing launch TSTO vehicles of this paper with the rocket TSTO vehicles of Ref. 6 under almost the same conditions.

The comparison shows that a vertical-launch-rocket TSTO vehicle, without the airbreathing engines, has the smallest dry mass, gross mass, and vehicle size. In addition, because of the difference in required landing gear the vertical launch vehicle is smaller than the horizontal takeoff vehicle.[6] Therefore, with respect to the masses, we conclude that the vertical-launch-rocket TSTO vehicle has the highest feasibility. However, the difference in total gross mass becomes less with increased payload capability. As a matter of course, we will have to evaluate reliability, cost, operability, and so forth before making a final decision regarding design. For instance, to horizontally launch horizontal landing vehicles is operationally easier than to launch them vertically. Another consideration is that airbreathing engines are probably more reliable than rocket engines.

For flight trajectories, the boosters accelerating with the aid of only rocket engines make simple flight histories like those of conventional rockets. On the other hand, the boosters with airbreathing engines require new guidance methods that will elicit the best performance of the airbreathing engines.

Conclusions

We applied an optimization method to the conceptual designs of airbreathing-launch two-stage-to-orbit (TSTO) space planes to find the smallest vehicles that can accomplish the mission requirements. The first-stage boosters in this study were classified into two types according to the propulsion systems: only airbreathing engines and airbreathing/rocket engines. First, the analysis tools were provided: the vehicle definition, the surface mesh generator, the aerodynamics analysis, the propulsion analysis, the mass estimation, and the trajectory analysis. Second, we integrated the analyses to specify the optimization problem. We defined the total dry mass of the first-stage booster and second-stage orbiter as a minimized parameter to find the best vehicle configurations and flight trajectories.

The results show that the TSTO space planes with boosters powered by both the airbreathing and rocket engines are lighter in total dry mass than vehicles with boosters propelled by only airbreathing engines. The difference under the payload requirement (between 0 Mg/0 m^3 and 8 Mg/80 m^3) is 19–37 Mg; the rate to the dry masses of the latter vehicle ranges from 7 to 33%. This study did not include incremental mass resulting from installing both of the airbreathing and rocket engines in a single vehicle. We need more accurate estimations of the component masses. In addition, the space planes are larger and heavier than existing airplanes and comparable expendable rockets. More mass reduction and miniaturization of components are necessary to increase the feasibility of the vehicles. Future studies should reconfirm the performance of the airbreathing engines and the mass estimation of vehicle components.

This study is characterized by its simultaneous optimization of the flight trajectories and vehicle configurations. The optimization demonstrates that the boosters can return to the launch site in the downranges caused by the ascent flights, using a nonlevel turn, long glide flight, and brief ignition of the airbreathing engines. It follows that the boosters consume little fuel in their return flight. Through this study, we confirmed that the proposed analysis and optimization method over the multiple disciplines were effective.

References

[1]Miyazawa, Y., Yanagihara, M., Sarae, W., Akimoto, T., Cretenet, J., and Bonnal, C., "HOPE-X High Speed Flight Demonstrator Research Program," *Proceedings of 22nd International Symposium on Space Technology and Science*, Japan Society for Aeronautical and Space Science, Motioka, Japan, 2000.

[2]Sato, T., Tanatsugu, N., and Naruo, Y., "Development Study on ATREX Engine," *Acta Astronautica*, Vol. 47, No. 11, 2000, pp. 799–808.

[3]Taguchi, H., Futamura, H., Yanagi, R., and Maita, M., "Analytical Study of Pre-Cooled Turbojet Engine for TSTO Spaceplane," AIAA Paper 2001-1838, April 2001.

[4]Maita, M., "Japan's TSTO Spaceplane Program," *5th World Aviation Congress*, Society of Automotive Engineers, San Diego, CA, 2000.

[5]Sobieszczanski-Sobieski, J., and Haftka, R. T., "Multidisciplinary Aerospace Design Optimization: Survey of Recent Developments," *Structural Optimization*, Vol. 14, No. 1, 1997, pp. 1–23.

[6]Tsuchiya, T., and Mori, T., "Optimal Conceptual Design of Two-Stage Reusable Rocket Vehicles Including Trajectory Optimization," *Journal of Spacecraft and Rockets*, Vol. 41, No. 5, 2004, pp. 770–778.

[7]Tsujimoto, T., Kouchiyama, J., and Shirouzu, M., "Current Status of the H-II Orbiting Plane Experimental (HOPE-X) Development," *Proceedings of 22nd International Symposium on Space Technology and Science*, Japan Society for Aeronautical and Space Science, Motioka, Japan, 2000.

[8]Morino, L., Chen, L., and Suciu, E., "Steady and Oscillatory Subsonic and Supersonic Aerodynamics around Complex Configurations," *AIAA Journal*, Vol. 13, No. 3, 1975, pp. 368–374.

[9]Raymer, D. P., *Aircraft Design: A Conceptual Approach*, AIAA, Reston, VA, 1999.

[10]Harloff, G. J., and Berkowitz, B. M., "HASA—Hypersonic Aerospace Sizing Analysis for Preliminary Design of Aerospace Vehicles," NASA CR-182226, Nov. 1988.

[11]Koelle, D. E., "TRANSCOST Statistical-Analytical Model for Cost Estimation and Economic Optimization of Space Transportation Systems," TCS-Trans Cost Systems, MBB Rept. URV-185(91), Ottobrunn, Germany, March 1991.

[12]Zipfel, P. H., *Modeling and Simulation of Aerospace Vehicle Dynamics*, AIAA, Reston, VA, 2000.

[13]Tsuchiya, T., and Suzuki, S., "Spaceplane Trajectory Optimization with Vehicle Size Analysis," *14th IFAC Symposium on Automatic Control in Aerospace*, International Federation of Automatic Control, Seoul, Republic of Korea, 1998, pp. 444–449.

[14]Harpold, J. C., and Graves, C. A., Jr., "Shuttle Entry Guidance," *Journal of the Astronautical Sciences*, Vol. 27, No. 3, 1979, pp. 239–268.

[15]NAL/NASDA HOPE Joint Research Team, "Aerodynamic Data Book-HOPE-X FY09," National Space Development Agency, NASDA TMR-000001, Tokyo, March 2000 (in Japanese).

[16]Tsuchiya, T., Mori, T., and Maita, M., "An Integrated Optimization for Conceptual Designs of Airbreathing Launch TSTO Vehicle," AIAA Paper 2001-1902, April 2001.

J. Martin
Associate Editor